Optical Engineering

OpticalEngineering.SPIEDigitalLibrary.org

Digital image correlation applied to the calculation of the out-of-plane deformation induced by the formation of roll waves in a non-Newtonian fluid

Alfredo Aranda
Nicolás Amigo
Christian Ihle
Aldo Tamburrino

SPIE.

Alfredo Aranda, Nicolás Amigo, Christian Ihle, Aldo Tamburrino, "Digital image correlation applied to the calculation of the out-of-plane deformation induced by the formation of roll waves in a non-Newtonian fluid," *Opt. Eng.* **55**(6), 064101 (2016), doi: 10.1117/1.OE.55.6.064101.

Digital image correlation applied to the calculation of the out-of-plane deformation induced by the formation of roll waves in a non-Newtonian fluid

Alfredo Aranda,[a,*] Nicolás Amigo,[a] Christian Ihle,[a,b] and Aldo Tamburrino[b,c]
[a]Universidad de Chile, Department of Mining Engineering, Tupper 2069, Santiago 8370451, Chile
[b]Universidad de Chile, Advanced Mining Technology Center, Blanco Encalada 2002, Santiago 8370449, Chile
[c]Universidad de Chile, Department of Civil Engineering, Blanco Encalada 2002, Santiago 8370449, Chile

Abstract. A method based on digital image correlation (DIC) is implemented for measuring the height of the roll waves developed in a non-Newtonian fluid flowing on an inclined channel. A projector and a high-resolution digital camera, placed vertically above the fluid surface, are used to project and record a random speckle pattern located on the free liquid surface, where the pattern is deformed due to the developed roll waves. According to the experimental geometry, the height of the roll waves associated to the out-of-plane deformation of the dots is obtained through a quantitative relationship between the experimental parameters and the in-plane displacement field in the flow direction. In terms of this, the out-of-plane deformation is found using a DIC criterion based on the speckle comparison between a reference image without the deformed pattern and an image with a deformed pattern. The maximum height of the roll waves computed with this technique is compared with the height measured using a lateral camera, with both results differing by <10% over the set of experimental instances. [DOI: 10.1117/1.OE.55.6.064101]

Keywords: deformation of liquid surface; digital image correlation; height scalar field in roll waves; non-Newtonian fluids.

Paper 160342 received Mar. 9, 2016; accepted for publication May 16, 2016; published online Jun. 1, 2016.

1 Introduction

The study and understanding of the surface waves developed in fluid flows are of essential importance for environmental as well as industrial applications, such as tailing flows and mudslides. For example, flows of Newtonian fluids in inclined channels frequently exhibit instabilities at their free surface.[1,2] In some cases, depending on the value of a Reynolds number written out of the flow depth, the fluid viscosity, and mean flow velocity, they evolve into roll waves. Liu and Mei[3] and later Huang and Garcia[4] have modeled this type of flow in two-dimensions and the laminar flow regime using boundary layer approximations when the (non-Newtonian) fluid is a Bingham plastic, i.e., has a yield stress and behaves as a Newtonian fluid in the limit of infinite shear rate (see also for an extension to Herschel–Bulkley fluids[5]). In an infinitely long channel, two flow zones are distinguished using this constitutive model. One, near the bottom with a parabolic velocity distribution. A second zone, connecting the parabolic velocity profile with the surface has a plug-shaped velocity profile,[4] which is almost constant. Roll waves in Bingham plastics depend on a critical Reynolds and, additionally on the yield stress via the Bingham number.[6] Several studies have been carried out in the field of theses waves both in channels and unconfined geometries.[7,8] The development of measurement techniques for roll waves is, therefore, as relevant as the understanding of their physical mechanism. Nowadays, there are many different optical techniques to visualize or measure the properties of fluid flows. For example, related to the approach discussed herein, some prominent techniques are the Schlieren effect, employed for the visualization of the flow of the natural convection in binary gas liquid-systems[9] and the new development of an optical instrument which allows the visualization of the discharge and distribution of fluids in the ambient bottom water;[10] the particle image velocimetry or particle tracking used to measure the particle dynamics in fluidized beds[11] and the velocity field for an indoor airflow;[12] and the Fourier Transform Profilometry to measure the deformation in and out-of-plane of a fluid.[13,14] In this study, a noninvasive technique to measure the height of roll waves using digital image correlation (DIC) for out-of-plane measurement is implemented and tested in a laboratory flume discharging a slurry. The method was first proposed by Pan et al.[15] and was validated by means of static geometric figures. Here, our aim is to apply this technique to identify the deformation of fluids in motion due to the propagation of roll waves. In this regard, the DIC method has the crucial advantage that it does not depend on the motion of the media, but on the exposure time of the camera. A prominent feature of this technique is that the height of the fluid can be measured regardless its physical conditions, such as temperature or sediment transport. Moreover, the experimental setup is simple, since only a high-resolution camera and the mechanical devices to fix it are required. As in particle image velocimetry, at least two images are needed in order to compare the deformed and undeformed projected pattern, which has a random distribution of dots. An important point to be outlined is that the technique has a limit of precision of 0.01 pixel in the displacement field,[16,17] thus allowing

*Address all correspondence to: Alfredo Aranda, E-mail: alfredo.arandan@gmail.com

measuring with considerable spatial resolution. The technique, by definition, requires the projection of a mask on a turbid surface, a requirement which is always fulfilled when studying open channel (either confined or unconfined) mudflows. The article is organized as follows. In Sec. 2, the principle of the DIC method and its equations are given. In Sec. 3, we show the experimental setup and the methodology. Then in Sec. 4, the results and discussion are presented. The conclusions are given in Sec. 5.

2 Principle of Digital Image Correlation Method

In the following section, we proceed to explain the basics of the DIC method, as well as their main equations.

2.1 *Out-of-Plane Height of a Liquid Surface*

The DIC method measures the in-plane deformation and displacement of the sample. However, it is possible to perform out-of-plane measurements using geometric equations which depend on the displacement field.[15] Figure 1 (adapted from Pan et al.[15]) shows the geometric scheme for a wave traveling in the $-x$ direction, where the image parameters depend solely on the spatial coordinates, valid for a given value of time. In the scheme, O_p and O_c represent the optic center of the projector and the camera, respectively, which focus the x plane. The l_p and l_c dotted lines indicate the distance from points O_p and O_c to the x plane, respectively. Point o is chosen randomly at the border of the digital image. The distances d_p and d_c separate the projector and the camera to the origin, respectively, where $d_p + d_c$ represents the distance between the projector and the camera. In order to determine the out-of-plane deformation, it is necessary to calculate the out-of-plane distance h, connecting the intersection of the segments $\bar{O}_cB$ and $\bar{O}_pA$ and the oX axis, as a function of variables that may be obtained directly from the geometry. From Fig. 1, we have the following equations

$$\tan\alpha = \frac{\Delta x_1}{h}, \tag{1}$$

$$\tan\beta = \frac{\Delta x_2}{h}. \tag{2}$$

On the other hand, we have

$$\tan\alpha = \frac{d_c + d_p - (\Delta x_1 + x + d_p)}{l_c - h} = \frac{d_c - \Delta x_1 - x}{l_c - h}, \tag{3}$$

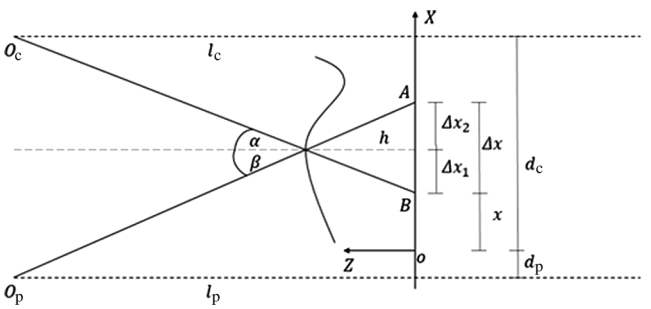

Fig. 1 Geometry employed to determine the out-of-plane displacement.

$$\tan\beta = \frac{\Delta x_1 + x + d_p}{l_p - h}. \tag{4}$$

Using Eqs. (1)–(2) and solving for h we obtain

$$h = \frac{\Delta x}{\frac{d_c}{l_c} + \frac{d_p}{l_p} + \left(\frac{1}{l_p} - \frac{1}{l_c}\right)x + \frac{1}{l_p}\Delta x}. \tag{5}$$

Following Pan et al.,[15] we define $x = Mu$, where M is the image magnification and u is the local displacement field in the x direction and at time t. Using the experimental setting $l_p = l_c$ and $M = 1$, Eq. (5) turns into the more convenient form

$$h = \frac{u}{\frac{d_c}{l_c} + \frac{d_p}{l_p} + \frac{1}{l_p}u}. \tag{6}$$

As it is seen in Eq. (6), the scalar height field is obtained by measuring the experimental parameters and the displacement field in the x direction, which is calculated from the DIC algorithm.

2.2 *Digital Image Correlation Using a Speckle Pattern*

DIC is an optical technique of a complete field, originally developed by Sutton et al.,[18] with which in-plane displacements and strains of the samples can be measured.[15,19,20] This technique is based on projecting a pattern on the surface of an object and capturing its initial and final deformed state, which are the called reference image and deformed image, respectively.[21] Typically, these images are obtained through a monochromatic CCD camera and they are digitally divided in a region of interest (ROI) containing a finite number of pixels[22] with the purpose of optimizing the computational correlation. The displacement field is calculated using a correlation algorithm which depends on the chosen criterion.[23] In this study, the zero-mean normalized cross-correlation, denoted as C_{ZNCC}, is shown[23] following the result achieved by Blaber et al.[24] for using an open-source MATLAB® algorithm. Optimal correlation using this algorithm requires values as close as possible to the unity

$$C_{ZNCC} = \frac{\sum[f(\tilde{x}_{ref_i}, \tilde{y}_{ref_j}) - f_m][g(\tilde{x}_{cur_i}, \tilde{y}_{cur_j}) - g_m]}{\sqrt{\sum[f(\tilde{x}_{ref_i}, \tilde{y}_{ref_j}) - f_m]^2[g(\tilde{x}_{cur_i}, \tilde{y}_c ur_j) - g_m]^2}}, \tag{7}$$

where f and g are the reference and deformed image grayscale intensity functions at a specified location (x, y), respectively. The functions f_m and g_m correspond to the mean grayscale values of the reference and current subset, which are indicated by

$$f_m = \frac{\sum f(\tilde{x}_{ref_i}, \tilde{y}_{ref_j})}{n(S)}, \tag{8}$$

$$g_m = \frac{\sum g(\tilde{x}_{cur_i}, \tilde{y}_{cur_j})}{n(S)}. \tag{9}$$

Here, $\tilde{x}_{\mathrm{ref}_i}$ and $\tilde{y}_{\mathrm{ref}_j}$ are the x and y coordinates of an initial reference subset point, and $\tilde{x}_{\mathrm{cur}_i}$ and $\tilde{y}_{\mathrm{cur}_j}$ are the x' and y' coordinates of a deformed subset of points, which are described by

$$\tilde{x}_{\mathrm{cur}_i} = x_{\mathrm{ref}_i} + u + \frac{\partial u}{\partial x}(x_{\mathrm{ref}_i} - x_{\mathrm{ref}_c}) + \frac{\partial u}{\partial y}(y_{\mathrm{ref}_j} - y_{\mathrm{ref}_c}), \tag{10}$$

$$\tilde{y}_{\mathrm{cur}_j} = y_{\mathrm{ref}_j} + v + \frac{\partial v}{\partial x}(x_{\mathrm{ref}_i} - x_{\mathrm{ref}_c}) + \frac{\partial v}{\partial y}(y_{\mathrm{ref}_j} - y_{\mathrm{ref}_c}). \tag{11}$$

The shape functions are identified from Eqs. (10) and (11), which relate the deformed geometric parameters with the reference geometric ones. From this functions, the searching vector parameter, p is defined [Eq. (12)], which is employed to determine the displacement field.[24]

$$\vec{p} = \left\{ uv \frac{\partial u}{\partial x} \frac{\partial u}{\partial y} \frac{\partial v}{\partial x} \frac{\partial v}{\partial y} \right\}^T. \tag{12}$$

The subscript c denotes the central point of the analyzed image and u and v are the displacement fields of the x and y directions, respectively. The deformation is characterized by the displacements u and v and their derivatives, which are constant for a given subset.[24] According to Pan,[25] there exists a relationship between the ZNCC and ZNSSD (zero-mean normalized sum of squared difference) criterion as in

$$C_{\mathrm{ZNSSD}} = 2(1 - C_{\mathrm{ZNCC}}), \tag{13}$$

where the C_{ZNSSD} criterion is usually employed because the optimization of the ZNSSD coefficient is relatively easier than that of the ZNCC coefficient.[25] This one is defined as follows:

$$C_{\mathrm{ZNSSD}} = \sum \left\{ \frac{f(\tilde{x}_{\mathrm{ref}_i}, \tilde{y}_{\mathrm{ref}_j}) - f_{\mathrm{m}}}{\sqrt{\sum [f(\tilde{x}_{\mathrm{ref}_i}, \tilde{y}_{\mathrm{ref}_j}) - f_{\mathrm{m}}]^2}} - \frac{g(\tilde{x}_{\mathrm{cur}_i}, \tilde{y}_{\mathrm{cur}_j}) - g_{\mathrm{m}}}{\sqrt{\sum [g(\tilde{x}_{\mathrm{cur}_i}, \tilde{y}_{\mathrm{cur}_j}) - g_{\mathrm{m}}]^2}} \right\}^2. \tag{14}$$

The DIC displacement resolution can be extended to 0.05 pixels by interpolating the correlation map to fractional locations of the pixels.[26] According to the resolution used in this study, this value corresponds to 4 μm. Furthermore, the biquintic B-splines developed by Blaber et al.[24] for the MATLAB® graphical user interface is employed in order to increase the calculation accuracy.

On the other hand, the mask, represented by the speckle pattern generated through an algorithm developed in MATLAB®, is projected on the fluid surface. The pattern has a spacial density of 7.3% which represents the space occupied by the white dots in the ROI whose dimensions are 42×42 pixels. This value is calculated with

$$\zeta = \frac{A_{\mathrm{s}} N_{\mathrm{s}}}{A_{\mathrm{c}}}, \tag{15}$$

where A_{s} is the area of a single dot (all dots have the same area), N_{s} is the number of dots which are in the subset, and A_{c} is the area of the subset. It is important to emphasize that with the chosen speckle pattern, a correlation coefficient >0.97 was obtained for all the images of this study.

3 Experimental Setup and Methodology

A scheme of the experimental setup used in this study is shown in Fig. 2. It consists of a 208.4×100.0 cm^2 plane base of melamine (impermeable to water), with a roughness small enough to allow a uniform flow of bentonite. This dark gray clay is completely turbid and, therefore, allowed the projection of the speckle pattern onto it. In the present set of experiments, a fixed concentration of bentonite of 11% by weight has been considered, which is shown in Fig. 3. Also, the tilting angle of the channel has been set to 7 deg and kept at this throughout the experiments. The corresponding rheology is of a 14.58 Pa yield stress and of a 0.089 Pa $\cdot$ s plastic viscosity, using the Bingham model. Two constant discharge volume flows have been made ($Q_1 = 79.3 \pm 1.7$ cm^3/s and $Q_2 = 171.7 \pm 1.9$ cm^3/s), whereas in both conditions a uniform laminar flow was obtained. The experiments were conducted at standard temperature and pressure conditions. On the metallic structure (2) a D3200 DSLR Nikon camera is placed to instantaneously capture the roll waves from above the flow, where frames have been exposed at 1/30 s. The speckle pattern has been projected on the flow using a BENQ model MS517F data projector and the dot diameter was ~4 pixels. On the plane base (1), a $190.0 \times 15.0 \times 1.7$ cm^3 melamine channel, fitted transparent polycarbonate walls have been installed. This allowed video recording of the lateral profile by an independent means. For this purpose, a Sony model DSC-WX300 digital camera has been used. The obtained images were digitalized to 8 bits and converted to grayscale. From the lateral images, an intensity threshold to discern the location of the free surface has been identified. On the other hand, (4) is a wood base, supporting the 19-cm diameter and 40-cm height acrylic tank (5), used for loading purposes. The latter is filled with a non-Newtonian liquid up to a 22 cm height. The fluid is discharged into the channel using a PVC tube (8), where two valves control the flow. The first one (7) controls the outflow of the tank and the inflow into the channel is regulated using (8). The flow is interrogated at point (2), where both the data projector and the overhead camera are installed. Finally, the fluid is recovered in the vessel (9). The measuring process is as follows. First, the video recorded is initiated (both the side and top view cameras). Then the valve for the outflow of the tank is opened and the flow is controlled with the inflow valve. After 5 s,

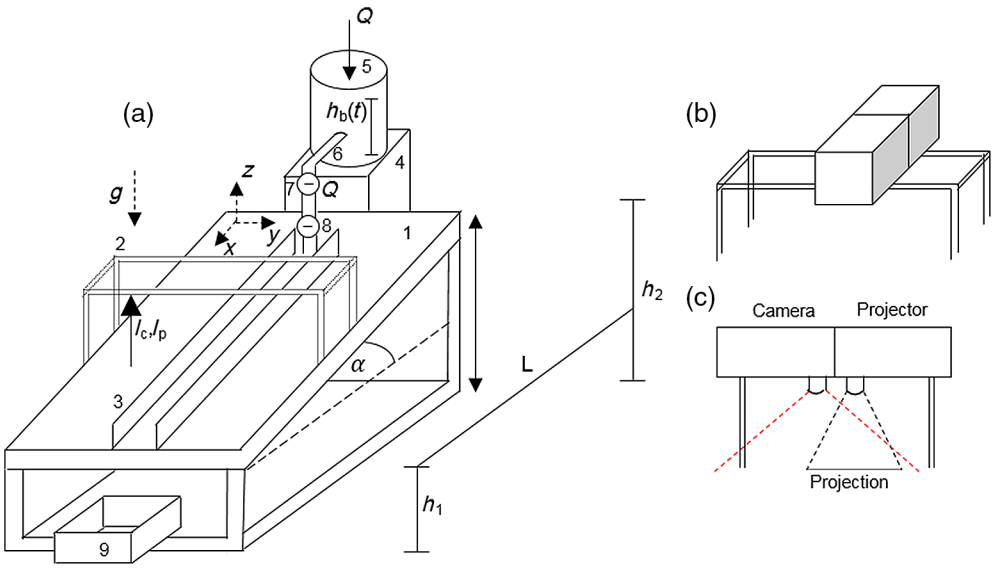

Fig. 2 Experimental setup. (a) Inclined channel on a melamine plane. (b) Projector and camera on the metallics structure. (c) Side view of the camera and the projector.

corresponding to the time required in order to reach a steady flow, eight images of different random roll waves are captured for a total of 18 waves. The process is repeated three times for the flow rate Q_1, obtaining a total of 24 images of the water–bentonite slurry. Then the process is repeated again for the flow rate Q_2, giving a total of 48 images. The two flow rates used during the experiments allowed to study two different velocities of wave propagation, thus testing the proposed measurement algorithm at these two different conditions. The calibration of the system was done using three opaque objects with dimensions of $10 \times 10 \times 0.5$ cm^3, $10 \times 10 \times 0.2$ cm^3, and $10 \times 10 \times 0.8$ cm^3 (width, length, and height). First, the speckle pattern was projected over the free-object surface. Then one of the objects was placed on the surface and the pattern was again projected over it. Thus, the measured height was obtained with the technique giving the following results: 0.494, 0.202, and 0.796 cm, respectively. From here, the factor of the calibration was calculated, obtaining a value close to 1 (0.99).

4 Results and Discussion

The DIC method is used to identify the out-of-plane deformation of roll waves developed using the Q_1 and Q_2. As the first step, it is necessary to capture the speckle pattern projected on the motionless fluid. Here, it is important to emphasize that the fluid does not flow at the set angle because the yield stress is greater than the gravitational force. This speckle pattern is shown in Fig. 4, and it is called the reference image, where it is noted that, due to the turbidity of the bentonite, the pattern penetrates about ~0.1 mm under the surface of the fluid, thus deeming distortions due to changes in optical properties between air and water irrelevant. In this section, we present the results of the DIC method and the calculated maximum heights of the roll waves for Q_1 and Q_2. Only one flow of each case is analyzed in detail.

Fig. 3 Fluid with a concentration of 11% of bentonite by weight.

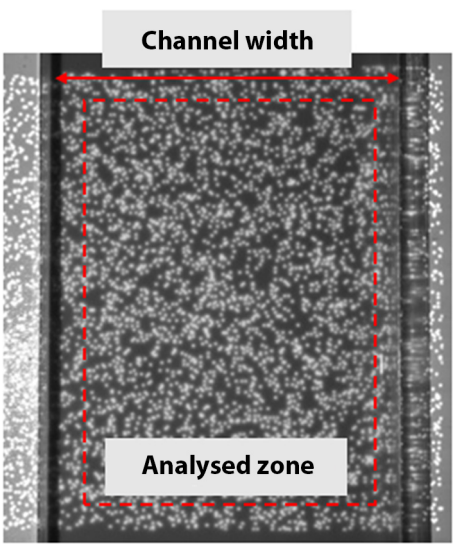

Fig. 4 Speckle pattern projected on the motionless fluid.

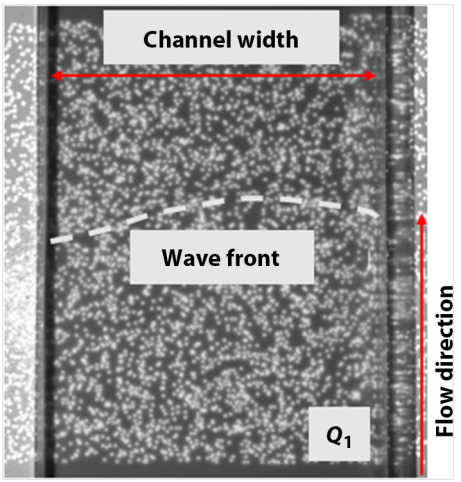

Fig. 5 Speckle pattern and the front wave identified in the Q_1 flow rate.

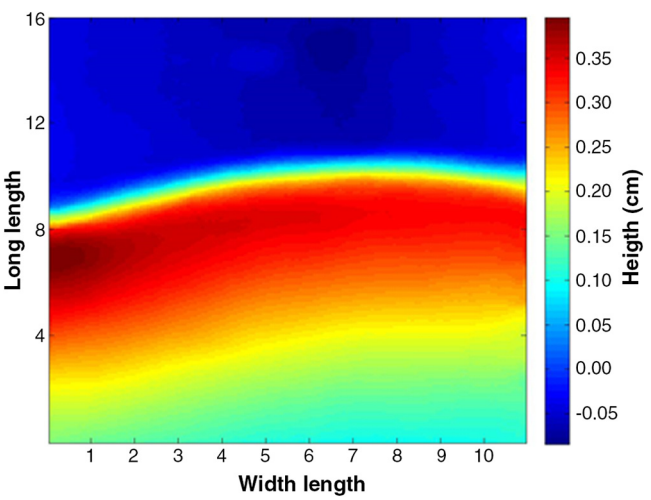

Fig. 6 Front wave and the height distribution of a roll wave in the Q_1 flow rate.

4.1 *Digital Image Correlation Applied to the Q_1 Flow Rate*

The DIC method is applied to the Q_1 flow rate. The speckle pattern projected on a roll wave is shown in Fig. 5, where the wave front is distinguished by analyzing the deformed pattern shown in Fig. 4. The displacement field in the wavefront direction is calculated using the DIC implementation proposed by Blaber et al.[24] To this purpose, the reference image is correlated with the deformed image in Fig. 5, allowing us to obtain the out-of-plane deformation presented in Fig. 6, where the height is represented by the color distribution. The maximum calculated height for this roll wave is obtained by adding the (constant) height field of the reference image (0.38 cm) to the calculated with the DIC technique, thus obtaining $h_{\mathrm{DIC}} = 0.97$ cm, which is indicated in the profile wave front shown in Fig. 7. This value is compared with the height measured using the lateral camera, h_{lat}, by capturing the wave front profile, which is observed in Fig. 8(a). In order to calculate h_{lat}, it is necessary to identify the position of the free surface, which is done by converting the image to a grayscale one and selecting one pixel with a prescribed threshold intensity. Figure 8(b) shows an example of the video-based measurement considering a threshold value of 0.404 of the grayscale (scale from 0 to 1) corresponding to the maximum height of the wave in the digital image. Thus, h_{lat} is equal to 0.92 cm, obtaining a percentage difference of 4.65%. The above process is repeated for different roll waves identified in the flow and their respective h_{DIC} and h_{lat} are summarized in Table 1. As can be seen, the calculated percentage differences are <10%, indicating that the heights obtained with the DIC method are in good agreement with those calculated using the lateral camera.

4.2 *Digital Image Correlation Applied to the Q_2 Flow Rate*

The previous analysis is repeated for the roll waves identified in the Q_2 flow rate. The same reference image of Fig. 4 has been used in this section. The speckle pattern projected on a roll wave is shown in Fig. 9, where the front wave is indicated. Again, this image is correlated with the reference image to calculate the displacement field and thus obtain

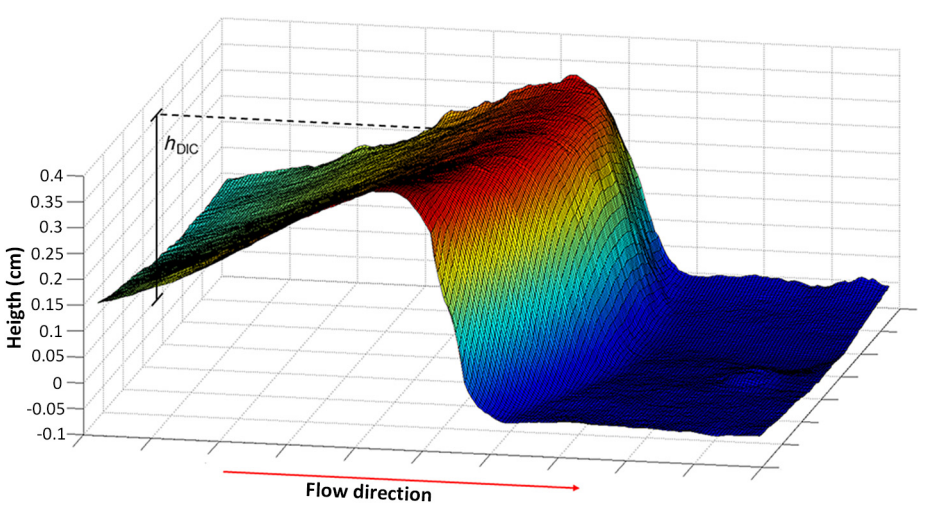

Fig. 7 Wave front profile and its maximum height for a roll wave in the Q_1 flow rate.

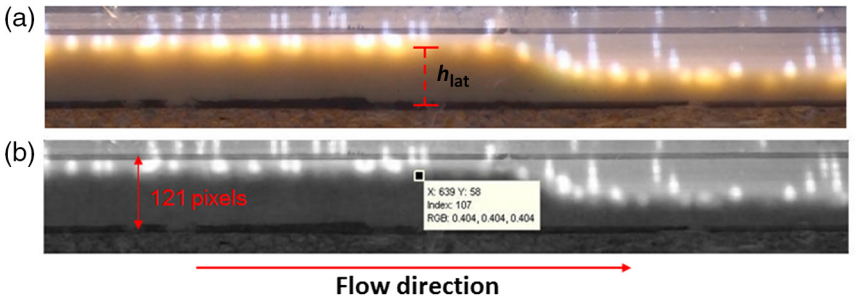

Fig. 8 Wave front profile of a roll wave in the Q_1 flow rate. (a) Captured image and (b) its gray-scale conversion.

Table 1 Maximum calculated h_{DIC} and h_{lat} heights and percentage differences for Q_1.

	Case 1			Case 2			Case 3		
Wave	h_{lat} (cm)	h_{DIC} (cm)	$\Delta_{\%}h$	h_{lat} (cm)	h_{DIC} (cm)	$\Delta_{\%}h$	h_{lat} (cm)	h_{DIC} (cm)	$\Delta_{\%}h$
1	0.75	0.78	3.22	0.86	0.90	4.87	0.97	0.92	4.65
2	0.79	0.77	2.48	0.74	0.70	5.17	0.81	0.77	4.65
3	0.83	0.79	4.16	0.84	0.91	7.57	0.85	0.82	4.42
4	0.84	0.81	2.71	0.83	0.81	1.47	0.72	0.71	0.98
5	0.81	0.78	3.58	0.86	0.83	4.00	0.60	0.58	3.61
6	0.67	0.67	0.60	0.80	0.78	2.82	0.75	0.73	2.73
7	0.85	0.83	2.41	0.97	0.98	1.63	0.75	0.72	4.01
8	0.79	0.80	1.25	0.84	0.84	0.12	0.68	0.63	6.95

the out-of-plane deformation, as shown in Fig. 10. In this case, the maximum calculated height for this roll wave is $h_{DIC} = 0.88$ cm, which is indicated in the profile wave front shown in Fig. 11. Measuring the maximum height using the captured image by the lateral camera, as seen in Fig. 12, we get $h_{lat} = 0.83$ cm. Hence, the percentage difference 5.36%. This analysis is repeated for different roll waves identified for this flow. The results are presented in Table 2, where the calculated percentage differences are <10%, as was already seen in the Q_1 case.

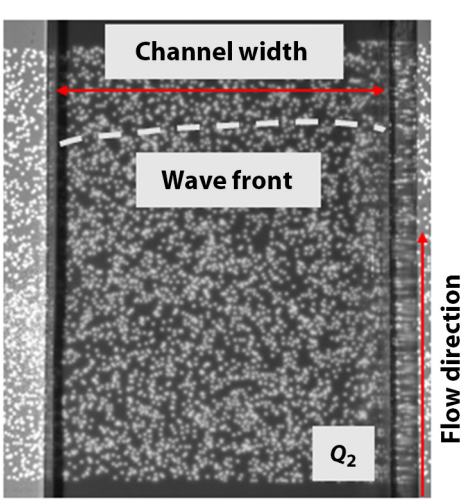

Fig. 9 Speckle pattern and the front wave identified in the Q_2 flow rate.

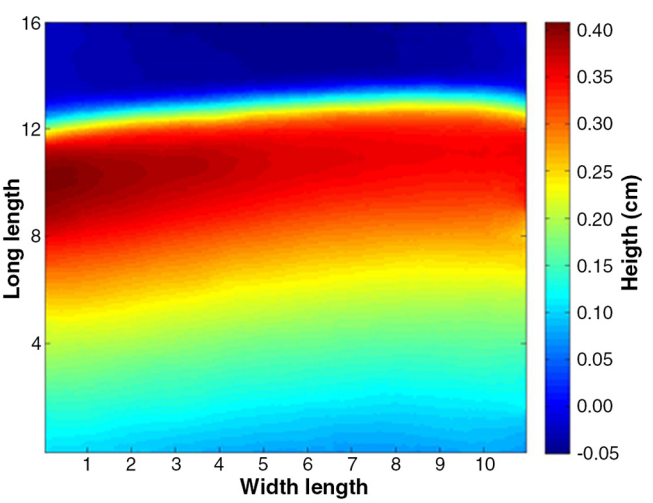

Fig. 10 Front wave and the height distribution of a roll wave in the Q_2 flow rate.

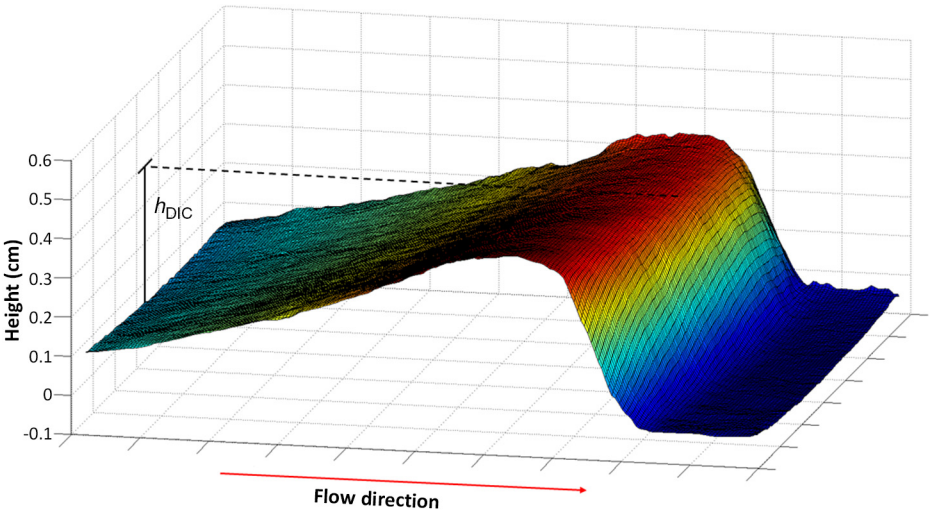

Fig. 11 Wave front profile and its maximum height for a roll wave in the Q_2 flow rate.

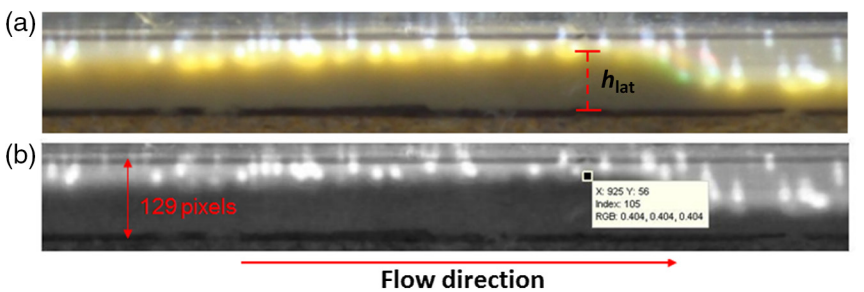

Fig. 12 Wave front profile of a roll wave in the Q_2 flow rate. (a) Captured image and (b) its gray-scale conversion.

Table 2 Maximum calculated h_{DIC} and h_{lat} heights and percentage differences for Q_2.

	Case 1			Case 2			Case 3		
Wave	h_{lat} (cm)	h_{DIC} (cm)	$\Delta_{\%}h$	h_{lat} (cm)	h_{DIC} (cm)	$\Delta_{\%}h$	h_{lat} (cm)	h_{DIC} (cm)	$\Delta_{\%}h$
1	0.79	0.79	0.38	0.74	0.72	2.65	0.71	0.72	1.25
2	0.78	0.79	0.63	0.78	0.83	5.21	0.77	0.77	0.00
3	0.81	0.83	2.65	0.68	0.68	0.29	0.83	0.84	1.43
4	0.83	0.88	5.36	0.74	0.72	2.21	0.83	0.83	0.24
5	0.74	0.75	1.21	0.72	0.71	1.41	0.77	0.78	2.04
6	0.77	0.78	2.04	0.78	0.77	0.26	0.78	0.82	4.98
7	0.76	0.81	5.59	0.75	0.77	2.84	0.70	0.74	5.03
8	0.75	0.79	4.45	0.78	0.79	1.77	0.82	0.79	3.79

5 Conclusions

In this study, the DIC was applied to analyze the out-of-plane deformation in turbid fluids, where it is possible to project a speckle mask on the surface. The maximum height of different roll waves developed on an inclined channel was calculated and the results were compared to the height obtained by using images captured by a lateral camera. Both results were in good agreement, which makes us presume that this technique is capable not only of calculating deformations in solids, as was already discussed by Gao et al.[27] and Pan et al.,[15] but also for calculating deformations in nontransparent fluids which are often encountered in different types of industries.

Furthermore, it was seen that the method was successfully applied for two different volumetric flow rates. Hence, the only limitation of capturing the images of the flow and then correlating them is the exposure time available in the camera. However, it has the advantage that any flow rate can be measured depending on the exposure time of the camera. Finally, we emphasize that the DIC method is a remarkably useful technique for measuring deformations in fluids, as well as solids, because it is noninvasive and its application does not depend on the physical conditions.

Acknowledgments

AA thanks CONICyT PhD fellowship No. 21140180, and NA thanks CONICyT PhD fellowship No. 21151448.

References

1. B. Benjamin, "Wave formation in laminar flow down an inclined plane," *J. Fluid Mech.* **2**(6), 554–573 (1957).
2. C. Yih, "Stability of liquid flow down an inclined plane," *J. Phys. Fluids* **6**(3), 321–334 (1963).
3. K. F. Liu and C. C. Mei, "Slow spreading of Bingham fluid on an inclined plane," *J. Fluid Mech.* **207**, 505–529 (1989).
4. X. Huang and M. H. Garcia, "A perturbation solution for Bingham-plastic mudflows," *J. Hydraul. Eng.* **123**(11), 986–994 (1997).
5. X. Huang and M. H. Garcia, "A Herschel–Bulkley model for mud flow down a slope," *J. Fluid Mech.* **374**, 305–333 (1998).
6. N. J. Balmforth and J. J. Liu, "Roll waves in mud," *J. Fluid Mech.* **519**, 33–54 (2004).
7. Z.-Y. Wang, "Free surface instability of non-Newtonian laminar flows," *J. Hydraul. Res.* **40**(4), 449–460 (2002).
8. E. Shapar, E. Kalaidin, and E. Demekhin, "On the solitary roll-waves on an inclined plane and their stability," *Thermophys. Aeromech.* **13**(1), 75–83 (2006).
9. A. Okhotsimskii and M. Hozawa, "Schlieren visualization of natural convection in binary gasliquid systems," *Chem. Eng. Sci.* **53**(14), 2547–2573 (1998).
10. V. Karpen, L. Thomsen, and E. Suess, "A new Schlieren technique application for fluid flow visualization at cold seep sites," *Mar. Geol.* **204**(12), 145–159 (2004).
11. T. Hagemeier et al., "Estimation of particle dynamics in 2-D fluidized beds using particle tracking velocimetry," *Particuology* **22**, 39–51 (2015).
12. S. Fu, P. H. Biwole, and C. Mathis, "Particle tracking velocimetry for indoor airflow field: a review," *Build. Environ.* **87**, 34–44 (2015).
13. P. Cobelli et al., "Global measurement of water waves by fourier transform profilometry," *Exp. Fluids* **46**(6), 1037–1047 (2009).
14. E. Zappa and G. Busca, "Static and dynamic features of Fourier transform profilometry: a review," *Opt. Lasers Eng.* **50**(8), 1140–1151 (2012).
15. B. Pan et al., "Improved speckle projection profilometry for out-of-plane shape measurement," *Appl. Opt.* **47**, 5527–5533 (2008).
16. H. W. Schreier, J. R. Braasch, and M. A. Sutton, "Systematic errors in digital image correlation caused by intensity interpolation," *Opt. Eng.* **39**(11), 2915–2921 (2000).
17. B. Pan et al., "Performance of sub-pixel registration algorithms in digital image correlation," *Meas. Sci. Technol.* **17**(6), 1615–1621 (2006).
18. M. Sutton et al., "Application of an optimized digital correlation method to planar deformation analysis," *Image Vision Comput.* **4**(3), 143–150 (1986).
19. K. Wang, M. Gao, and A. Tieu, "Volume-grating digital speckle pattern interferometry for measurement of dynamic out-of-plane displacement fields," *Measurement* **43**(4), 479–482 (2010).
20. H. Hu et al., "Digital speckle based strain measurement system for forming limit diagram prediction," *Opt. Lasers Eng.* **55**, 12–21 (2014).
21. Y. H. Huang et al., "Shape measurement by the use of digital image correlation," *Opt. Eng.* **44**(8), 087011 (2005).
22. J. Zhao et al., "Initial guess by improved population-based intelligent algorithms for large inter-frame deformation measurement using digital image correlation," *Opt. Lasers Eng.* **50**(3), 473–490 (2012).
23. B. Pan, "Recent progress in digital image correlation," *Exp. Mech.* **51**(7), 1223–1235 (2011).
24. J. Blaber, B. Adair, and A. Antoniou, "Ncorr: open-source 2-D digital image correlation MATLAB software," *Exp. Mech.* **55**(6), 1105–1122 (2015).
25. B. Pan, H. Xie, and Z. Wang, "Equivalence of digital image correlation criteria for pattern matching," *Appl. Opt.* **49**, 5501–5509 (2010).
26. Z. Liu et al., "Transmission-speckle correlation for measuring dynamic deformation of liquid surface," *Opt. Lasers Eng.* **65**, 110–116 (2015).
27. J. Gao, W. Xua, and J. Geng, "3-D shape reconstruction of teeth by shadow speckle correlation method," *Opt. Lasers Eng.* **44**(5), 455–465 (2006).

Biographies for the authors are not available.